A STUDY ON THE FABRICATION AND CHARACTERIZATION OF SPUTTERED Cr DOPED ZnO THIN FILM GAS SENSORS

NAIF HAMMAD MISSHIN AL-HARDAN

UNIVERSITI SAINS MALAYSIA

2011

A STUDY ON THE FABRICATION AND Characterization of Sputtered Cr DOPED ZnO THIN FILM GAS SENSORS

By

NAIF HAMMAD MISSHIN AL-HARDAN

Thesis submitted in fulfillment of the

requirements for the degree of

Doctor of Philosophy

June 2011

ACKNOWLEDGEMENTS

First, I am heartily thankful to my supervisor Professor Dr. Mat Johar Bin Abdullah, whose encouragement, guidance and support from the initial to the final level enabled me to develop an understanding of the subject. My thankful also goes to Associate Professor Dr. Azlan Abdul Aziz the co-advisor to this work with their valued advice and patient that rose in several published works.

I would like to take this opportunity to thank the N.O.R. and the solid-state laboratory staffs for their generous help and technical support offered during my laboratorial work and for their assistance in the characterizations for the samples. My thanks also go to the FE-SEM laboratory staff at the School of Biological Sciences-USM.

I would like to acknowledge the approval for continuing my Ph.D reading from the ministry of science and technology (MOST) – Iraq. The USM fellowship program is highly appreciated. I would also like to gratefully acknowledge all staff members of the School of Physics of their encouragement.

My grateful thanks go to my family members, my wife and kids for their patient during my research, my mother for her pray and brothers for their encouragement.

Lastly, I offer my regards to all of those who supported me in any respect during the completion of the project, my colleges in solid-state lab and NOR lab within these 4 years of this research time.

Naif Al-Hardan

Penang – Malaysia

TABLE OF CONTENTS

ACKNOWLEDGEMENTS ii

TABLE OF CONTENTS iii

LIST OF TABLES vi

LIST OF FIGURES vii

LIST OF SYMBOLS xi

LIST OF MAJOR ABBREVIATIONS xii

ABSTRAK xiii

ABSTRACT xiv

CHAPTER 1 – INTRODUCTION 1

1.1 Introduction 1

1.2 The objective 4

CHAPTER 2 - FUNDAMETALS OF ZINC OXIDE GAS SENSORS 5

2.1 Introduction 5

2.1.1 Growing of ZnO 8

2.2 A Review of ZnO Gas Sensor 11

2.3 Energy Band Structure of Metal Oxide 15

2.4 Metal – Semiconductor Contacts **16**

2.5 The effect of oxygen chemisorptions on the surface states **19**

2.6 The Sensing Mechanisms **22**

CHAPTER 3 - EXPERIMENTAL TECHNIQUES **27**

3.1 Fabrication of the sensors **27**

3.1.1 The ZnO and Cr doped ZnO sensing material **30**

3.2 Characterization techniques **33**

3.2.1 X-ray diffraction **33**

3.2.2 Field Emission Scanning Electron Microscope (FESEM) **34**

3.2.3 Atomic Force Microscope **35**

3.2.4 Energy dispersive X-ray spectroscopy (EDS or EDX) **36**

3.2.5 Impedance spectroscopy (IS) **36**

3.3 The gas sensor performance **40**

3.3.1 Experimental setup **40**

3.3.2 Gas delivery system **43**

3.3.3 The Gas Sensor Parameters **45**

CHAPTER 4 - RESULTS AND DISCUSSION **49**

4.1 The performance of the heating elements **49**

4.2 Structure and morphology of the undoped and Cr doped ZnO **51**

4.3 The Effect of Cr doping on the sheet resistance of ZnO films **62**

4.4 The metal – semiconductor behavior of the gas sensor **68**

4.5 The effect of Cr doping on the operating temperature of ZnO gas sensor **79**

4.6 The undoped and doped ZnO gas sensor. **85**

4.6.1 The stability of ZnO gas sensor. **85**

4.6.2 The gas sensing performance of undoped and 1at% Cr:ZnO **86**

4.6.2.1 Oxygen sensing performance of the undoped and doped ZnO **87**

4.6.2.2 The performance of the undoped and doped ZnO under reducing gas atmosphere **92**

4.6.2.2 (a) The response for acetone vapors **92**

4.6.2.2 (b) The sensor response for hydrogen gas **100**

4.7 The evaluation of oxygen species **104**

4.7.1 Oxygen gas **104**

4.7.2 Acetone vapor **105**

4.8 The effect of 1at% Cr doping on the response time of the ZnO gas sensors **107**

4.9 The sensing mechanisms of the undoped and 1at% Cr doped ZnO gas sensor **108**

CHAPTER 5 - CONCLUSIONS AND FUTURE WORK **114**

APPENDICES **116**

Appendix A - The Surface Space Charge Model **116**

Appendix B - Impedance Spectroscopy **119**

REFERENCES **122**

LIST OF PUBLICATIONS BASED ON RESEARCH WORK **139**

LIST OF TABLES

Table 1.1:	Show some flammable gases of interest [7, 16].	2
Table 3.1:	The RCA procedures for Si cleaning.	28
Table 4.1	The Cr concentration, c-axis and the strain of Cr-doped ZnO.	54
Table 4.2:	Grain size and the surface roughness (rms) of the prepared ZnO films.	58
Table 4.3:	The E_L and E_H of Cr doped ZnO films	67
Table 4.4 :	The fitting values for the complex impedance of ZnO sensor at different temperatures.	78
Table 4.5:	R_g, R_{gb}, and C_{gb} of the undoped ZnO sensor for different O_2 concentrations.	90
Table 4.6 :	R_g, R_{gb}, and C_{gb} of the 1 at% Cr doped ZnO sensor for different O_2 concentrations.	92
Table 4.7 :	The fitting values for the complex impedance of the undoped ZnO sensor.	99
Table 4.8 :	The fitting values for the complex impedance of 1at% Cr doped ZnO sensor.	100
Table 4.9 :	The fitting parameters for the complex impedance of the undoped ZnO sensor under different H_2 concentrations.	103

LIST OF FIGURES

Figure 1.1	**Commercially available gas sensor and research prototypes gas sensors [26, 28].**	4
Figure 2.1	**Unit cell of the ZnO crystal structure [39].**	8
Figure 2.2	**The schematic of a typical RF sputtering unit.**	10
Figure 2.3	**The schematic of band structure in (a) metal, (b) semiconductor and (c) insulators [79].**	16
Figure 2.4	**Energy band diagrams of a metal and n-type semiconductor before and after contact [83].**	18
Figure 2.5	**The band model of MOS before the oxygen adsorption (a), and after the equilibrium state of oxygen adsorption (b) [4, 7, 84].**	20
Figure 2.6	**The oxygen spices detected at different temperatures of SnO_2 surface by different techniques (IR= Infrared spectroscopy, TPD = Temperature programmed desorption, EPR = Electron paramagnetic resonance) [1].**	26
Figure 3.1	**Process steps for the fabrication of the ZnO gas sensors.**	31
Figure 3.2	**Device Layout of the gas sensor.**	32
Figure 3.3	**The optical (a) and the SEM (b) image of the prepared gas sensor.**	33
Figure 3.4	**Visualization of the Bragg equation [105].**	34
Figure 3.5	**A simple RC parallel circuit [114].**	38
Figure 3.6	**The complex impedance characterization of an ideal resistor and a capacitor in parallel [114].**	39
Figure 3.7	**The schematic measurement setup for gas sensor characterization.**	41
Figure 3.8	**The impedance characterization of a single RC and a pair of RC.**	42
Figure 3.9	**The I-V characteristics of a 50 Ω resistor**	42
Figure 3.10	**The gas test chamber and the gas sensor under test.**	43
Figure 3.11	**The side view of the gas test chamber.**	44
Figure 3.12	**The experiment setup for the VOC test**	46
Figure 3.13	**The resistance, the response time and the recovery time for a typical gas sensor [1].**	48
Figure 3.14	**The image of the experimental setup (1) the gas sensor, (2) the gas test chamber, (3) the mass flow meter, (4) SMU 237, (5) DMM 196, (6) DC power supply for the heating element, (7) the impedance analyzer, (8) DMM 2100, (9) gas cylinders and (10) PC with GPIB and Lab View software.**	48

Figure 4.1	**The calibration curve of the heating element.**	50
Figure 4.2	**Operating temperature of the heating element in long run.**	50
Figure 4.3	**XRD pattern of the undoped and Cr doped ZnO.**	52
Figure 4.4	**The effect of Cr concentrations on the Bragg angle of (002) peak and d spacing of the prepared ZnO films.**	55
Figure 4.5	**The EDS spectra of 4at% Cr doped ZnO on Si wafer substrate.**	55
Figure 4.6	**3D AFM image of the undoped ZnO (a) and Cr doped ZnO with 1 at.% (b), 2 at.% (c), 3 at.% (d) and 4 at.% (e).**	57
Figure 4.7	**FE-SEM of the prepared ZnO before (a) and after annealing (b) and of doped with Cr at 1 at.% (c), 2 at.% (d), 3 at.% (e) and 4 at.% (f). The left hand side of the image is at (x50k), the middle is (x100k) and right side hand is at (x150k).**	61
Figure 4.8	**The electrical resistance behavior of undoped and Cr doped ZnO as a function of operating temperature.**	62
Figure 4.9	**The resistance of Cr doped ZnO at different concentrations at 350 ^{o}C.**	64
Figure 4.10	**Ln σ vs ($k_{\beta}T$)-1 of the undoped and doped ZnO.**	65
Figure 4.11	**The activation energy of the undoped and doped ZnO films prepared by RF sputtering.**	67
Figure 4.12	**The I-V behavior of the Pt/ZnO/Pt, before and after annealing at 500 ^{o}C for 6 hr.**	68
Figure 4.13	**The I-V characteristics of Pt/ZnO/Pt at the temperatures from RT to 500 ^{o}C.**	69
Figure 4.14	**The I-V behavior of the Pt/ZnO:Cr/Pt, at operating temperature of 300 ^{o}C; Cr concentration is 1at%.**	71
Figure 4.15	**The complex impedance of Pt/ZnO/Pt device structure as a function of temperature.**	72
Figure 4.16	**The real (a) and imaginary (b) part of the impedance as a function of log *f* at different operating temperatures.**	74
Figure 4.17	**Electric modulus of the sample impedance at room temperature.**	77
Figure 4.18	**The experimental and the fitting curve of the proposed model of the sample's impedance. The proposed model of the sample's equivalent circuit is shown in the inset.**	79
Figure 4.19	**The response of undoped ZnO and Cr doped ZnO sensor as a function of operating temperature for various gases; (a) ethanol, (b) isopropanol, (c) acetone and (d) hydrogen.**	82
Figure 4.20	**The sensitivity of ZnO sensor as a function of Cr concentrations.**	83

Figure 4.21	**The dependence of the sensor response on operating temperatures of doped and undoped ZnO sensor for 50% O_2 gas.**	84
Figure 4.22	**The resistance stability of the (a) doped and (b) undoped ZnO sensor at operating temperature 400 ^oC and 300 ^oC respectively.**	86
Figure 4.23	**The dynamic response of undoped ZnO sensor at operating temperature 350 ^oC for different O_2 concentrations.**	87
Figure 4.24	**The dynamic response of Cr-doped ZnO sensor at operating temperature 250 ^oC for different O_2 concentrations.**	88
Figure 4.25	**The repeatability of the Cr-doped ZnO sensor in sensing 50% O_2 at 250 ^oC.**	88
Figure 4.26	**Nyquist plot of undoped ZnO for different O_2 concentrations at 350 ^oC. The symbols represent the experimental data, while the lines represent the modeling curve.**	89
Figure 4.27	**Nyquist plot of Cr doped ZnO for different O_2 concentrations operated at 250 ^oC. The symbols represent the experimental data, whereas the lines represent the modeling curve.**	91
Figure 4.28	**The response of the undoped ZnO sensor when exposed to acetone, Isopropanol and ethanol at concentration of 500 ppm measured individually. The operating temperature was fixed at 400 ^oC.**	93
Figure 4.29	**The response of the prepared ZnO gas sensors for different acetone concentration at operating temperature 400 ^oC.**	94
Figure 4.30	**The response repeatability of the undoped ZnO sensor in acetone sensing at 400 ^oC.**	94
Figure 4.31	**The response of the 1at% Cr doped ZnO sensor when exposed to acetone, Isopropanol and ethanol at concentration of 500 ppm measured individually. The operating temperature was fixed at 300 ^oC.**	95
Figure 4.32	**The response of the 1at% Cr doped ZnO gas sensors for different acetone concentration at operating temperature 300 ^oC.**	96
Figure 4.33	**The repeatability of the 1at% Cr doped ZnO sensor in sensing 500 ppm acetone at 300 ^oC.**	96
Figure 4.34	**Nyquist plot of the undoped ZnO sensor at 400 ^oC for different acetone concentration. The symbols represent the experimental data, while the lines represent the modeling curve.**	97
Figure 4.35	**Electric modulus plot for the data taken at 400 ^oC with 500 ppm acetone concentration.**	98
Figure 4.36	**Nyquist plot of 1at% Cr doped ZnO sensor for different acetone concentration. The fitting curves show complete semicircles using the data of table (4.8).**	100

Figure 4.37	**The response of the undoped ZnO gas sensors for different H_2 concentration at operating temperature of 400 ^oC.**	102
Figure 4.38	**The response of the doped ZnO gas sensors for different H_2 concentration at operating temperature of 350 ^oC.**	102
Figure 4.39	**Nyquist plot of the undoped ZnO sensor at 400 ^oC for different H_2 concentration. The symbols represent the experimental data while the lines represent the fitting curve.**	103
Figure 4.40	**Resistance of the undoped and 1% Cr doped ZnO sensor when exposed to O_2 at different concentration levels at the operating temperatures of 350 ^oC and 250 ^oC respectively.**	105
Figure 4.41	**Resistance of undope and 1% Cr doped ZnO sensor when exposed to acetone at different concentration levels at the operating temperatures of 400 ^oC and 300 ^oC respectively.**	106
Figure 4.42	**The barrier height at the grain boundaries of the undoped ZnO (a) before reaction and (b) after the reaction with reducing gases. The upper section and lower section represents the physical model and the band model respectively.**	109
Figure 4.43	**The barrier height at the grain boundaries of the Cr doped ZnO (a) before reaction and (b) after the reaction with reducing gases. The upper section and lower section represents the physical model and the band model respectively.**	110
Figure 4.44	**The cross section layout of the prepared ZnO sensor.**	112
Figure 4.45	**The schematic of the prepared ZnO gas sensor and the corresponding model of an equivalent circuit.**	112

LIST OF SYMBOLS

q	Charge of an electron
E_{CB}	Conduction band energy level
E_F	Fermi level of semiconductor
E_{Fm}	Fermi level of metal
E_{gap}	Semiconductor band gap
E_{VB}	Valence band energy level
I	Electric current
k	Boltzmann constant
R	Resistance
T	Absolute temperature
V	Voltage
θ	X-ray diffraction angle
ρ	Resistivity
σ	Conductivity
Φ_B	Schottky barrier height
Φ_m	Metal work function
Φ_s	Semiconductor work function
χ	Electron affinity

LIST OF MAJOR ABBREVIATIONS

AFM	Atomic Force Microscopy
a. u.	Arbitrary Unit
C_{gb}	Grain Boundary Capacitance
EDX	Energy Dispersive X-ray analysis
FESEM	Field Emission Scanning Electron Microscopy
IS	Impedance Spectroscopy
I-V	Current-Voltage
MOS	Metal Oxide Semiconductors
MSM	Metal-Semiconductor-Metal
RCA	Radio Corporation of America
RF	Radio Frequency
R_g	Grain Resistance
R_{gb}	Grain Boundary Resistance
rms	Root mean square
XRD	X-Ray Diffraction
VOC	Volatile Organic Compounds

Kajian Tentang Fabrikasi dan pencirian Penderia Gas Filem Nipis Terpercik ZnO Terdop Cr

ABSTRAK

Filem nipis zink oksida (ZnO) dan ZnO terdop kromium (Cr) telah berjaya dihasilkan melalui percikan bersama frekuensi radio secara reaktif dari sasaran logam kromium dan zink berketulenan tinggi. Kepekatan Cr berada dalam julat peratusan atom (1 - 4). Pembelauan sinar- X mendedahkan bahawa filem ZnO mempunyai struktur polihabluran dengan fasa dominan (002) tumbuh sepanjang paksi c dari struktur heksagon ZnO tersebut. Puncak (002) teranjak sedikit ke sudut Bragg lebih tinggi ketika Cr menggantikan Zn dalam hablur ZnO. Filem mempamerkan butiran nano tertabur seragam dengan struktur turus.

Penderia gas berasaskan filem ZnO tak terdop dan terdop Cr difabrikasikan yang merangkumi platinum / tantalum sebagai elektrod dan elemen pemanas. Ciri-ciri dan prestasi penderia gas diukur dan dinilai melalui pengukuran arus – voltan, sambutan rintangan – masa dan spektroskopi impedans di bawah persekitaran gas yang berbeza (oksigen, hidrogen dan sebatian organik meruap sperti aseton, etanol, dan isopropanol. Penderia gas berasaskan ZnO terdop Cr mempamerkan sambutan lebih tinggi pada suhu operasi yang lebih rendah 250 ^{o}C bagi oksigen dan 300 ^{o}C bagi wap VOC berbanding dengan yang ditunjukkan oleh ZnO tak terdop suhu operasi adalah 350 ^{o}C bagi okigen dan 400 ^{o}C bagi wap VOC. Keputusan ini dijelaskan dan dibincangkan dalam kaitannya dengan struktur permukaan penderia gas dan kesan selanjutnya pada prestasi penderia tersebut. Spektroskopi impedans dari penderia mendedahkan bahawa sambutan penderia boleh dikaitkan dengan rintangan sempadan butiran yang sekali lagi mencadangkan pentingnya kereaktifan permukaan penderia dalam penderiaan gas.

Akhirnya, penderia menunjukkan kestabilan yang baik dengan prestasi boleh ulang semula dalam kepekatan gas yang berbeza. Penderia gas ZnO terdop Cr mempamerkan sambutan lebih tinggi dan masa sambutan lebih pantas berbanding dengan yang dipamerkan penderia gas ZnO tak terdop.

A Study on the Fabrication and Characterization of Sputtered Cr doped ZnO Thin Film Gas Sensors

ABSTRACT

Zinc oxide (ZnO) and chromium (Cr) doped ZnO thin films were successfully produced by reactive radio frequency co-sputtering of high purity zinc and chromium metal targets. The Cr concentrations were in the range of (1 – 4) atomic percentage. The X – ray diffraction revealed that the ZnO films possessed a polycrystalline structure with a (002) dominant phase grown along the c-axis of the hexagonal structure of the ZnO. The (002) peak was slightly shifted toward higher Bragg angles when the Cr substitutionally replaced the Zn in the ZnO crystals. The films exhibited a uniformly distributed nano grains with a columnar structure.

Gas sensors based on the undoped and Cr doped ZnO films were fabricated that incorporated platinum/tantalum as electrodes and heating element. The characteristics and performance of the gas sensors were measured and evaluated through current – voltage, resistance – time response and impedance spectroscopy measurements under different gas environment oxygen, hydrogen and volatile organic compound such as acetone, ethanol and isopropanol. The gas sensor based on Cr doped ZnO exhibited higher response at lower operating temperature (250 ^{o}C and 300 ^{o}C for oxygen and VOC vapors respectively) as compared to that of the undoped (the operating temperatures were 350 ^{o}C and 400 ^{o}C for oxygen and VOC vapors respectively). The result was explained and discussed in relation to the gas sensor's surface structure and its subsequent effect on the sensor's performance. Impedance spectroscopy of the sensor revealed that the sensor's response was attributed to the grain boundary's resistance which again suggests the significance of the sensor's surface reactivity in the gas sensing.

Finally, the sensors showed a good stability with reproducible performance in different gas concentration. The Cr doped ZnO gas sensor exhibited a higher response and faster response time as compared to that of the undoped ZnO gas sensor.

CHAPTER 1
INTRODUCTION

1.1 Introduction

The development of gas sensors to monitor the toxic and combustible gases is imperative due to the concerns for environmental pollution and the safety requirements for the industry. The sensors and sensors arrays are also used in medical applications, automotive and process control. In general, sensors provide an interface between the electronic equipment and the physical world typically by converting non electrical of physical or chemical quantities into electrical signals. Recently, gas sensors based on the semiconducting metal-oxides (they also are known as resistive or chemoresistive sensors) such as tin dioxide (SnO_2), zinc oxide (ZnO) and tungsten trioxide (WO_3) were found to be very useful for detecting the toxic, harmful and hydrocarbons gases [1-7].

Volatile organic compound (VOC) vapors are the primary sources of indoor environmental pollutants and are considered seriously harmful to the human body [8, 9]. Notable correlations between VOC emissions and different kinds of cancers have been reported [10]. Therefore more work is needed concerning the vapors effects and its detection process [10-14]. Among the VOC, acetone is widely used in many applications, notably as biomarker for diabetes since it can be found in the exhaled breath of the diabetes patient.

Gas chromatography and mass spectrometry are the most prevalent among the available techniques for analyzing VOCs in the air [15]. However, they are expensive, bulky, and unable to perform in situ and continuous measurements.

Table 1.1 presented some flammable gases of interest in air mixtures [7, 16].

Table 1.1 Show some flammable gases of interest [7, 16]

Gas	Lower explosive limit (LEL) (vol%)
Hydrogen	4.0
Ethane	3.0
Propane	2.1
Butane	1.8
Ethanol	5.5
Kerosene	0.7

The fundamental sensing principle relies on the change of conductivity of the sensing material when they are exposed to certain target gases at certain temperatures. The change is usually proportional to the concentration of the gas. There are two types of metal oxide sensors: n-type such as ZnO, SnO_2, titanium dioxide (TiO_2) and ferric oxide (Fe_2O_3) and p-type such as nickel oxide (NiO), cobalt oxide (Co_2O_3). Both types of sensors may response to reducing and oxidizing gases [7, 17].

Metal oxide gas sensors were discovered a long time ago, where the effect of the ambient atmosphere on the electrical conductance of semiconductors was described by pioneers such as Barttain and Bardeen [18], Heiland [19] and Seiyama and co-workers [20]; the discovery of these behaviors became commercialized at the beginning of 1960s by Taguchi [21] .

Since then researches and technical developments have been extensively applied to enhance the sensing properties of the produced metal oxide gas sensors.

The understanding of the sensing phenomena has been approached from different views that have been summarized [22-24]. First by the basic research scientists that applied different techniques to determine the simplified model of the sensor operation, second by the developers who empirically optimize the preparation and test procedures and lastly by the users of the sensors who test and described the sensors' parameters (sensitivity, selectivity and stability). In these steps different instrumentations have been applied, some of them were simples such as digital multimeter, others are more complicated, which needs more consumable time such as spectrometers.

In spite of many researches involve in the improvement of the metal oxide semiconductors' gas sensors, still there is a need to reduce the operating temperature and enhance both the sensitivity and selectivity of the sensors.

The most analyzed gas sensors in the past was based SnO_2 [25-28] and ZnO [29-33]. These semiconducting metal-oxides exhibit good sensitivity to oxidizing and / or reducing gases, but they also present unsatisfactory selectivity, reproducibility, thermal stability and durability. Many other metal oxide semiconductors have also been studied extensively and their behaviors could be found in many published articles [7].

The sensors consist mainly of sensing semiconductor material coated over a suitable electrodes, an insulator substrate such as a thick alumina substrate or a silicon wafer with an insulator layer of silicon dioxide (SiO_2) or silicon nitride (SiN_x) and a suitable heater that is isolated from the electrode [22].

Commercially, companies still used a thick alumina as a substrate [34, 35], and many research centers are trying to use the silicon as it can be used in the IC

manufacturing process [36, 37]. Figure 1.1 depicts different type of gas sensors as commercially product and research prototypes.

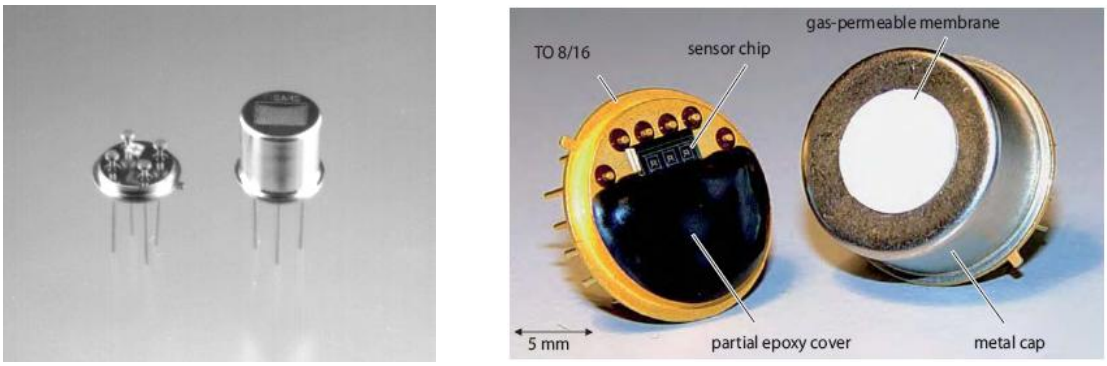

(a) Commercial product **(b) Research prototypes**

Figure 1.1 Commercially available gas sensor and research prototypes gas sensors [34, 36]

Previous work revealed that gas sensors based on thin films ZnO were operating at high temperatures [38, 39]. For power saving, longer life time and reliability of the operation, low operating temperature of the gas sensors is desirable. Doping ZnO with various metals was shown to reduce the sensor's operating temperature and improved its response [40-42].

1.2 The objective

In view of the need for the a better gas sensor, the main objective of this study is to fabricate the Cr doped ZnO thin film gas sensors by co- reactive RF sputtering of high – purity Zn and Cr metal targets. To the best of our knowledge, we believe that the effect of Cr doping on the RF sputtering ZnO thin films for gas sensing applications has not been published before.

Embarking as this objective, the structural properties of the films will be studied in relation to their electrical properties upon subjected to gas (O_2, H_2 and VOC) environments. Extensive impedance measurement will be performed to elucidate the contribution of different components of the gas sensors towards the observed electrical response in these gases atmosphere.

CHAPTER 2

FUNDAMETALS OF ZINC OXIDE GAS SENSORS

2.1 Introduction

Zinc oxide (ZnO) became a material of interest for a variety of electronic applications. It can be used in a large number of areas and unlike many of the materials with which it competes, ZnO is inexpensive, relatively abundant, chemically stable, easy to prepare, and non-toxic. Most of the doping materials that are used with ZnO are also readily available. According to a new report from NanoMarkets [43], devices and materials based on ZnO are expected to create major new opportunities for the electronics industry over the next few years ranging from enhanced antistatic coatings to high-value-added products such as solid-state lighting and display backplanes. The report predicts that revenues from the leading ZnO related electronics applications will reach about US $ 860 million in 2012, rising to US $ 2.3 billion in 2016, which was around US $ 500 million in 2009 -2010 according to the same report. The study also stresses that despite the economic recession, ZnO electronics will generate new business revenues, because it addresses real world problems in a cost effective way. ZnO is a unique material that combines the virtues of a material that is easily and inexpensively obtained and whose basic properties are well understood with the ability to serve in important future applications within electronics and optoelectronics.

ZnO is an inorganic material and belongs to II-VI compound semiconductors. It is considered a wide band semiconductor with a direct band gap of approximately 3.3 eV at 300K, i.e. near the ultraviolet (UV) region of the electromagnetic spectrum,

for a hexagonal (wurtzite) type structure. It exists in nature by mineral name of “zincite” with yellow to red color depending on the amount of the impurities, specially the manganese (Mn). Due to its large band gap, ZnO is colorless and clear. The material is considered to be an n-type; this behavior is attributed to the oxygen deficiency in the material structure [44, 45].

ZnO has attracted the research interest since the 1930s, and then peaked around the end of the 1970s and the beginning of the 1980s. The interest then faded away, partly because it was impossible to dope ZnO with both n and p-type, and partly because of the interest moved to other compounds such as gallium nitride (GaN) and gallium arsenide (GaAs), that have been used in low dimensional structures applications such as quantum wells. The research on ZnO first initially focused on the bulk samples of ZnO such as growing process, doping, band structures and electrical transport [46-48].

Another interesting wave of ZnO began in the mid of the 1990s, where it was documented in conference, workshops and symposia that more than 2000 related papers were published in 2005 as compared to 100 publications in the 1970s [47]. The number of these papers exceeds 2000 per year during the last 5 to 10 years as indicated e.g. by the databases INSPEC or web of science [48].

The recent interesting development of the ZnO is based on the possibility to grow the compound by epitaxial layers, quantum wells, nanorods, quantum dots and related objects, where research were focused on the applications of the ZnO as [44, 45, 48, 49]:

- A blue/UV optoelectronics, including light emitting diodes, laser diodes instead of using the GaN and SiC based structures.

- A ferromagnetic material by doping it with cobalt (Co), manganese (Mn), Iron (Fe), vanadium (V), etc. for semiconductor spintronics.

- Highly transparent conducting oxides by doping with aluminum (Al), gallium (Ga), indium (In), etc. as an alternative to In-SnO (indium tin oxide ITO).

ZnO has been used commercially as varistors that constitute hundreds of millions of dollars business a year. ZnO based surface wave acoustic devices are also regularly used in mobile phones [43].

For the above applications, many published works deal with the preparation of undoped and doped ZnO that has led to the research been focused on the nanostructures (structures with a reduced dimension) emphasizing on the electrical and optical properties. The large exiton energy of the ZnO (about 60 meV) comparing to the GaN (26 meV) and ZnSe (22 meV) [50] has given more advantage to this compound in the optoelectronic applications, at room temperature and higher temperatures.

Figure 2.1 shows the hexagonal wurtzite type structure of the ZnO. The c-axis is chosen to be parallel to z, while the a and b – axis is laid in the x-y plane with equal length and an angle of 120^{o}. One Zn ion is surrounded tetrahedrally by four O ions and the similarly for the oxygen ions. Each primitive unit cell is consisting of two formula unit of ZnO. The value of the lattice constant at room temperature is a = b ~ 0.3249 nm while for the c is about 0.5206 nm. The ZnO grows preferably in the hexagonal type structure. However, the compound may be grown as a zincblend cubic structure on a suitable cubic substrate, and a rocksalt structure under high pressure. The later structures are both form the face cubic center (fcc), but with different atoms arrangements [44, 48].

ZnO is an ionic bond compound. According to the ionic bound of the ZnO, the bottom of the conduction band is formed from the 4s levels of the Zn^{2+} and the top of the valance band from the 2p levels of the O^{2-}. The gap between the bottom of the conduction band and the top of the valance band is around 3.437 eV at low temperatures [51].

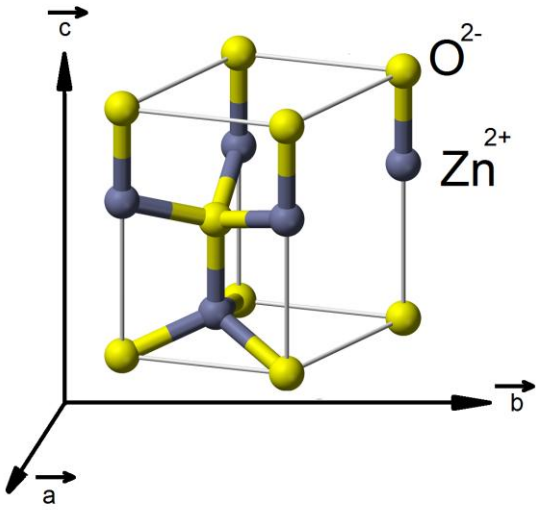

Figure 2.1 Unit cell of the ZnO crystal structure [47]

2.1.1 Growing of ZnO

For scientific and technical applications many growing methods had been used to prepare high quality of ZnO single crystals, thick films as well as thin films [44, 49, 52], such as molecular beam epitaxy, hydrothermal growth for single crystal and screen printing for thick films. Thin films form of ZnO had been most attractive since they led to the size reduction of the prepared device. These methods include spin coating, chemical vapor deposition (CVD) and pulse laser deposition (PLD). One of the most popular growth techniques during the early ZnO investigations was the sputtering (direct current (DC) sputtering, radio frequency (RF) magnetron

sputtering and reactive sputtering) [49, 52]. The sputtering methods draw the attention of many research groups for many reasons such as low cost, simplicity, and low operating temperature. The quality of the resulted films appears to be reasonably good. Here we focused on the RF reactive sputtering since it is the process that had been used in this study. The RF sputtering yield reproducible thin films characterizations.

RF reactive sputtering is considered as one of the physical vapor deposition (PVD) since in this method, there is no chemical reaction as a starting material. The sputtering process usually works at moderate vacuum around 2 x 10^{-2} millibar (mbar) where the pressure of the sputtering gas is maintained stable. The unit is consisting of the following main components as it is shown in Figure 2.2. The target is fixed with the material to be used on the cooled surface of the anode. The substrate holder is where the substrate to be coated is fixed. The radio frequency generator is used to ignite the plasma inside the chamber at a constant frequency of typically 13.56 MHz [52].

Argon (Ar) is used as a sputtering gas, since it is inert; in the process the atom's gas is ionized and bombarded target’s material. The different potential between the target (anode) and the substrate holder (cathode) make the sputtered ions causes towards the substrate. This process can be used to sputter the material from metals and insulators.

In the reactive sputtering method, the main gas (Ar) is accompanied by other gas, which is known as a reactive gas such as oxygen or nitrogen where there will be a reaction between the sputtered material and the reactive gas. This process is used in producing ZnO from the sputtering of the Zn metal with the reactive oxygen gas. It is

believed as preferable method since the stoichiometry of the prepared compound can be better controlled [49, 53].

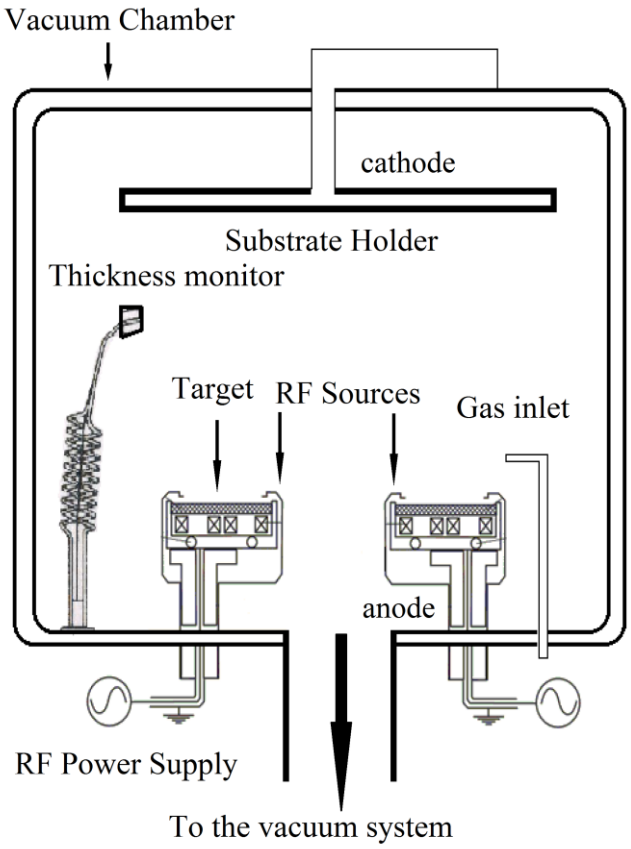

Figure 2.2 The schematic of a typical RF sputtering unit.

Most of the published works of the ZnO prepared by reactive RF sputtering showed high quality samples and highly preferred c-axis orientation of the (002) phase of the hexagonal wurtzite structure as detected by the X ray diffraction [52, 54].

2.2 A Review of ZnO Gas Sensor

ZnO has some interesting properties that is able to create opportunities as a component for gas sensor and biosensor [49, 55]. It has been studied extensively for gas sensing application, since Heiland [19] reported the influence of ambient gas on the electrical conductivity of a ZnO single crystal. Seiyama et al. [20] reported for the first time the gas sensing behavior of a thin film form of ZnO. Later, many published works reported on this application and recently on the ZnO nanostructure as a successful candidate for gas sensing applications [56-59]. Despite many published works on this subject, ZnO gas sensor appears to show a high operating temperature as well as low response, which may not be as attractive as commercialized tin oxide (SnO_2) gas sensor. Nevertheless, ZnO is still a good candidate for gas sensor applications since it is readily fabricated into thin film by various techniques.

ZnO gas sensor has been fabricated by different methods in different forms (single crystals, thick films and thin films), namely sputtering DC and RF sputtering [56, 60], Sol-gel [57], pulse laser deposition [61], and metal organic chemical vapor deposition (MOCVD) [62].

Different gases such as hydrogen (H_2) [60, 63], hydrocarbons such as ethanol (C_2H_6O), methanol (CH_3OH), Methane (CH_4) liquefied petroleum gas (LPG)) [7], ammonia (NH_3) [64], and carbon monoxide (CO) [31], which are considered as reducing gases; another type of gases, which consider as oxidizing gas such as ozone (O_3) [65], nitrous (NO_x) [66] and oxygen (O_2) [67] have also been investigated as testing gas for these gas sensors.

Weichsel et al. [62] prepared ZnO single crystal on GaAs substrate by MOCVD and palladium was used to form a Schottky contact. The current at reverse bias was found to increase as the ambient atmosphere switched to H_2 gas, indicating a detectable response to H_2 gas. The device was able to recover fully to the initial state at room temperature after 17 hours. Kim et al. [68] used commercial ZnO single crystal to prepare a Schottky diode with platinum (Pt) contact. The current–voltage (I –V) behavior under different H_2 concentration was studied, and it showed an increase in the measured current as the H_2 concentration was increased. Here, the behavior was non-reversible, suggesting that the H_2 was introduced as shallow donors into the ZnO. The electrical conductivity of ZnO single crystals have been investigated by Bott et al. [69] in response to CO, methane (CH_4), and H_2 in air mixtures at temperature range from 300° to 500 °C. The ZnO single crystal showed a response to H_2 and CO with the maximum response at the temperature of around 400 °C with a response time of about 2 minutes, but it was insensitive to CH_4.

Thin films of ZnO are attractive since they are low cost, reproducible and compatible with the modern IC technology process. ZnO thin films for gas sensors have been studied by many groups to sense different gases such as H_2 [39, 60], C_2H_6O, CH_3OH, CH_4, LPG [7], NH_3 [64], and CO [31], O_3 [65], NO_x [66] and O_2 [67].

The gas sensing properties of ZnO thin films deposited on a glass slide by sol gel was studied by Musat et al. [57]. The gas sensor response towered O_3 gas was activated by UV light, thus allowing the sensor to work at room temperature. The work revealed that gas-sensing response was strongly depended on the porosity and the grain size of the polycrystalline films. Min et al. [39] prepared ZnO gas sensors on silicon (Si) substrates where the effect of the different ratio of the reactive to the

sputtered gas was studied. The operating temperature of the sensor in detecting gases such as H_2, NO_2 and CO were found to fall in the range of 350 to 450 ^oC

The improvement of ZnO gas sensor sensitivity had been achieved by the addition of dopants such as aluminum (Al), indium (In), copper (Cu), iron (Fe), tin (Sn), antimony (Sb) and bismuth (Bi) into the ZnO thin film. The amount and the type of dopant were found to modify the sensitivity of the sensor, especially due to Sn and Al [70, 71]. The improvement of gas sensing properties and the operating temperature of the ZnO have also been demonstrated by using the metal catalysts such as palladium (Pd), Pt, rhenium (Rh), silver (Ag) and gold (Au) [72]. The use of metal catalyst raises a problem of the diffusion of those metals into the platform (silicon substrate) of the sensors. For example, Pt can introduce deep level traps in the band gap of silicon that act as efficient recombination centers, causing high junction leakage to the outside boundary of the devices [64, 73].

The enhancement of the ZnO response was also demonstrated through the change in the surface states of the ZnO material as reported by Law and Thong [64] who suggested a way of increasing the sensitivity of a ZnO nanowire by reducing the carrier concentration. The carrier concentration was controlled through reducing and oxidizing gas plasma. Al-Hardan et al. [29] proposed an alternative low cost method to reduce the carrier concentration of ZnO thin films. By controlling the oxidation time of Zn thin film, the electronic surface states were modified and the electron concentration could be varied. The study demonstrated the increased response of the sensor for low concentration of H_2 gas.

The most important factors affecting sensing properties, especially the response is the grain size [74-78]. The response of ZnO nanostructure gas sensor was

relatively high that was attributed to the grain-size effect. That increases the surface area of the sensor. Recent studies were focused on the correlation of surface and interface topology with deposition parameters and physical properties of the sensing materials [3, 79]. Thus understanding the correlation of microstructure with the electrical properties of ZnO thin films is essential.

Various structures of ZnO had been grown by different methods and their physical properties have been studied extensively. The effect of different types of nanostructures such as Nanobelts [80, 81] nanowires [82], tetrapods [83], nanorods and nanopillar [84] of ZnO has been studied for gas sensing applications. Choopun et al. [80] prepared nanobelts of ZnO by RF sputtering and studied their response towards ethanol sensing at operating temperatures in the range of 200 ^{o}C to 290 ^{o}C. A single crystal nanobelt was prepared by Xu et al. [81] to detect NH_3 by I-V measurement and impedance spectroscopy techniques. Pd was used to form a Schottky contact that showed non linear I-V behavior. Hongsith et al. [82] prepared ZnO gas sensor from nanowires by oxidation of Zn metal powder and doped with Au. The prepared sensor was tested for C_2H_6O at optimum operating temperature of around 240 ^{o}C. A three-dimensional network of ZnO tetrapods was fabricated by Delaunay et al. [83], through thermal oxidation of Zn powder and was used for C_2H_6O sensing at various concentration with optimum operating temperature of 400 ^{o}C. ZnO nanopillar gas sensor was used in sensing C_2H_6O and H_2 with optimum operating temperature of 400 ^{o}C [84]. Sol gel ZnO nanocrystalline based gas sensor showed the highest sensitivity towards C_2H_6O at operating temperature of 250 ^{o}C [85].

2.3 Energy Band Structure of Metal Oxide

Metal Oxide Semiconductors (MOS) such as ZnO and SnO gas sensors are considered as semiconductor materials, characterized with a moderate electrical conductivity. To contribute to the conductivity, electrons should overcome the amount of energy equivalent to the energy band gap (E_{gap})

$$E_{gap} = E_{CB} - E_{VB} \tag{2.1}$$

where E_{CB}, the bottom of the conduction band energy level and E_{VB}, is the upper of the valence band energy level.

Metal such as Al, Cu and Pt has high electrical conductivity, since its conduction band is partially filled or overlaps the valance band. The uppermost electrons in the valance band can move to the next band freely with just a small amount of energy. For the insulator material that is known to have a wide energy band gap such as diamond and silicon dioxide (SiO_2), the electrons occupied the valance band are highly bonded to the band, whereas the conduction band is totally empty of electrons. At high external energy (thermal or electric filed) the electrons may move to the empty conduction bands through the large energy band gap but the current of the electrons can be considered negligible. For semiconductor materials with the conductivity lies between that of metal and insulator, the conduction band is partially occupied by the electrons at room temperature where the thermal energy is sufficient to excite the weak bounded electrons from the upper valance band to the bottom of the conduction band. This is because of the narrow energy band gap of the semiconductor materials which in the case of Si is about 1.1 eV and for the ZnO, it is 3.37 eV. The simplified schematic energy band structure is shown in Figure 2.3.

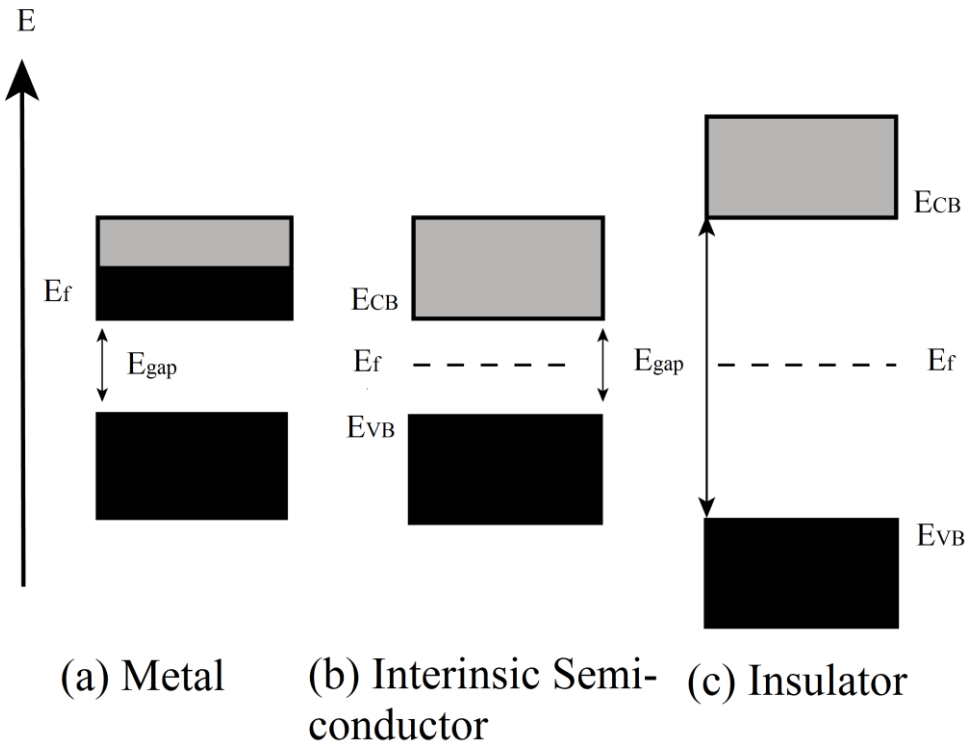

Figure 2.3 The schematic of band structure in (a) metal, (b) semiconductor and (c) insulators [86].

In semiconductor materials, the electrons mostly have the probability of occupying an energy level that lies in the middle of the energy gap, known as Fermi level (E_F) [87, 88]. The level is raised to beneath the conduction band for the n-type semiconductors or above the valance band in the case of the p – type semiconductors.

2.4 Metal – Semiconductor Contacts

The metal – semiconductor contact may be rectifying or non-rectifying, which will depend on the barrier height at the interface between the semiconductor and the metal been used. For simplicity, here an n-type semiconductor will be considered, since the ZnO is an n-type semiconductor [44, 45, 49]. A metal – semiconductor junction can be formed by depositing a metal over the semiconductor or depositing

the semiconductor over the pre-coated metal. Figure 2.4 shows the ideal energy band diagrams of a metal and an n-type semiconductor before and after contact.

The metal – semiconductor contacts may form ether an Ohmic contact where the current flows equally in both directions of the contacts or Schottky contact where there will be a rectification. Those behaviors depend on the energy band configuration between the two components. Energy of Φ_m (metal work function) and Φ_s (semiconductor work function) is required to free an electron from the metal and the semiconductor respectively. The energy required for removing an electron from the bottom of the conduction band of a semiconductor is known as electron affinity (χ_S).

For Schottky contact with an n-type semiconductor, the work function of the metal is higher than that of the semiconductor. When the metal and the semiconductor are brought together, the Fermi level of these materials will be at the same level in equilibrium. If the work function difference of the two materials is significant, the barrier heights of the metal - semiconductor contact is significant. The contact is known as Schottky contact that shows a rectification current behavior. On the other hand if the work function difference is not significant, the current will show an Ohmic behavior. The mechanism for carrier transport at the junctions is known as thermionic emission if the contact is Schottky contact and as tunneling and field emission if it is Ohmic contact. It is to be noted also that the doping concentration plays a significant role in determining the behavior of the currents.

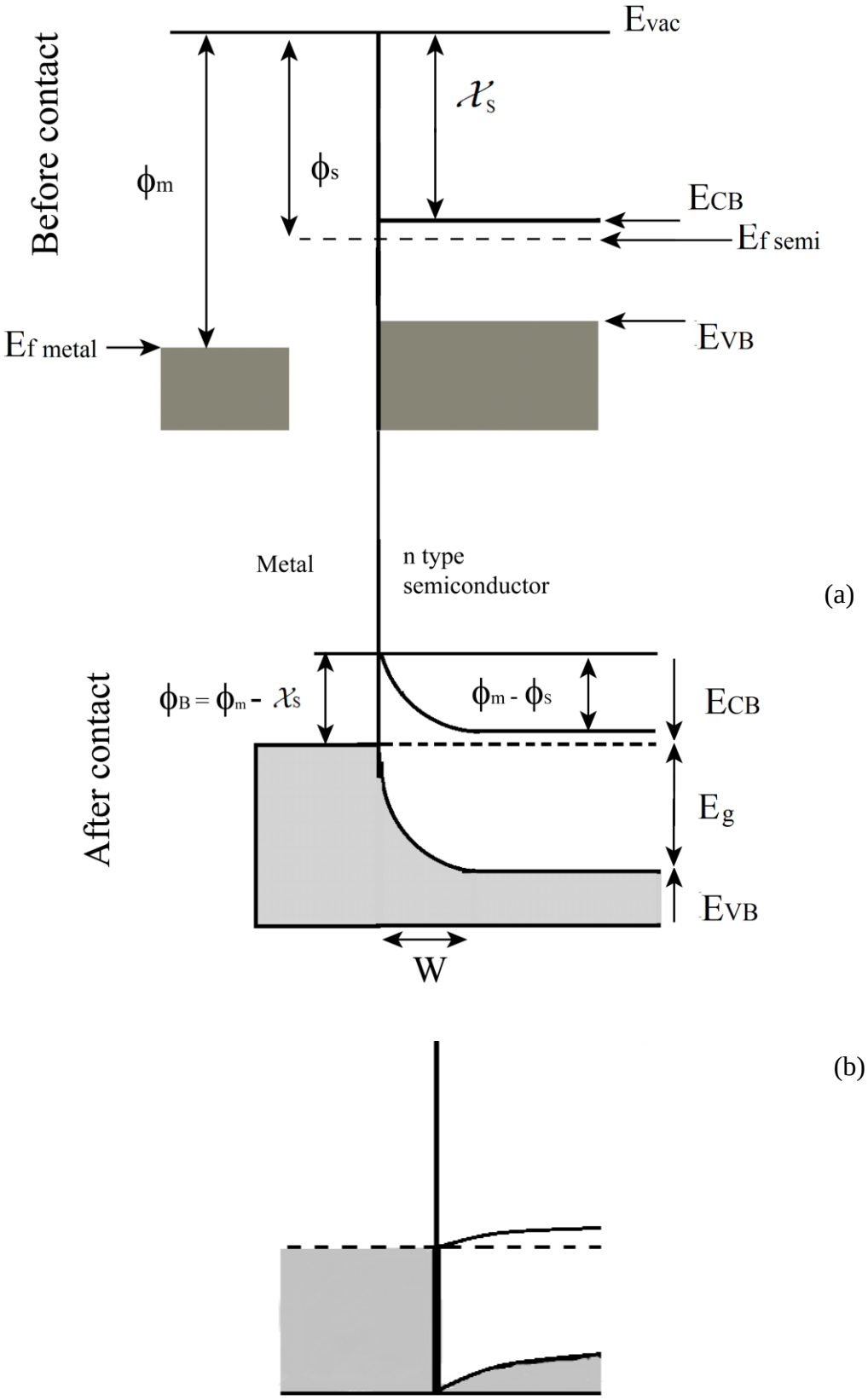

Figure 2.4 Energy band diagrams of a metal and n-type semiconductor before and after contact [89] (a) Schottky contact, (b) Ohmic contact.

2.5 The effect of oxygen chemisorptions on the surface states

The charge transfer in a chemisorptions process is very important in the understanding of gas sensing mechanisms as most of the process occurs at the surface of a MOS. The surface between the MOS and a gas is referred to as a free surface or just a surface, while the surface between the MOS and another solid is usually referred to as an interface [2, 4, 7].

The concept can be clarified as follow and is shown schematically in Figure 2.5. Initially, a neutral surface state is shown in Figure 2.5. At the surface of the MOS, the periodicity of the crystal structure is broken, leading to dangling bonds, which are unsaturated sites. This will result in the generation of new energy levels, known as surface states [4, 7]. Figure 2.5a shows the MOS surface is in flat band condition, which there is no charge exchange between the surface states and the semiconductor [90]. These sites can act as a donor or acceptor type. The position of the surface state relative to the Fermi level of the MOS depends on its affinity to the electrons, and for the n-type MOS this will be high and the surface state act as acceptors. After oxygen molecules from the atmosphere are chemisorbed, it will attracts the electrons from the conduction band and the band bending occurs that will create the surface barrier (known also as Schottky barrier height) of qV_s (Figure 2.5b), and an electron depleted layer is formed, which is also known as a space charge layer x_o. This will lead to a reduction in the conductivity (increasing the resistivity) of the MOS surface. The band edge bending of the conduction band and of the valance band is related to the change of the surface charges. It is to be noticed that the adsorbed oxygen species do not only come from the gas phase, but could

also emerge from the lattice sites, as thermal decomposition of the MOS may lead to the co- existence of the vacancies and adsorbed species. [91].

The band bending can be described by means of 1D Poisson equation [4, 23] [Appendix A].

$$\frac{\partial^2 V_{(x)}}{\partial x^2} = -\frac{\rho}{\varepsilon_S} \tag{2.2}$$

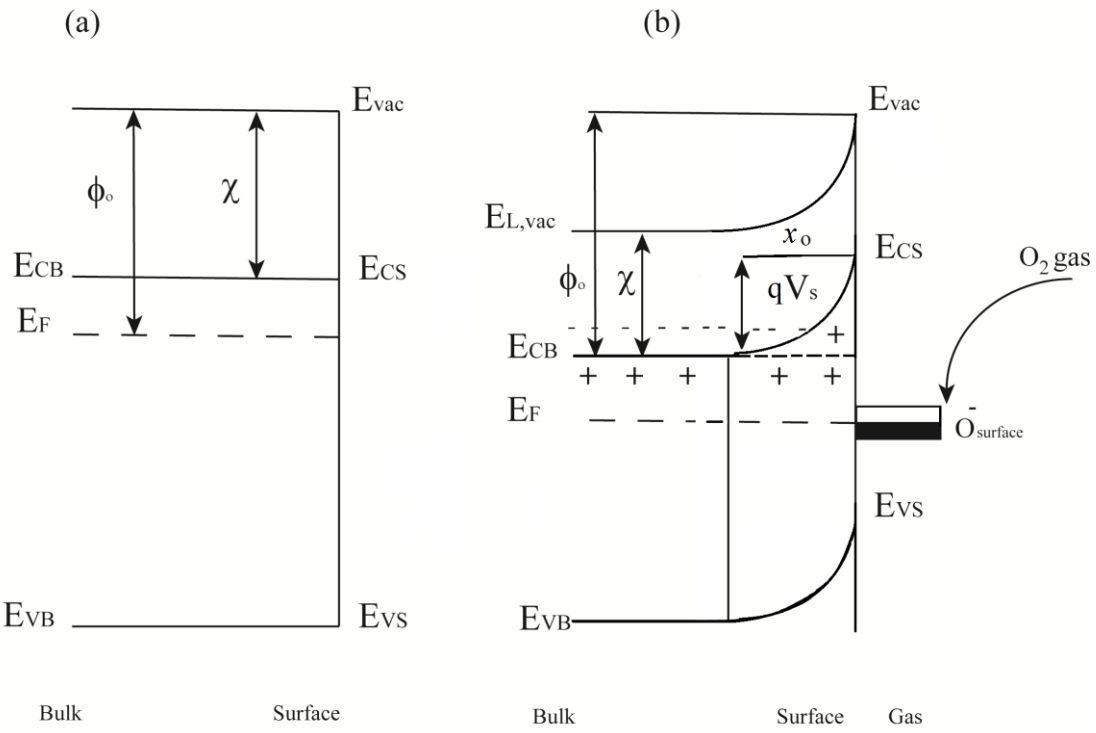

Captions: E_{vac} is the vacuum level
E_{CB}, E_{VB} are the conduction and the valance band energy level of the MOS bulk
E_{CS}, E_{VS} are the conduction and the valance band energy level of the MOS surface
E_F is the Fermi level
ϕ_o and χ are the work function and the electron affinity.
The (-) and (+) represents the electrons and the donor sites respectively

Figure 2.5 The band model of the MOS before the oxygen adsorption (a), and after the equilibrium state of the oxygen adsorption (b) [4, 7, 90].

where $V_{(x)}$ the electric potential, ρ the charge density in the bulk, x a distance from the surface into the bulk and ε_S is the permittivity of the semiconductor. Since the position of the surface state for the n-type MOS is below the Fermi level (acceptor levels), this will cause the extraction of the electrons by the oxygen molecules from the MOS, and the space charge region is formed at the surface. The band bending leads to the limitation of oxygen adsorption on the surface, as the surface acceptor (oxygen) reached the electrochemical potential of the bulk that caused no further chemisorption process. This equilibrium process is known as "Weisz limitation", which describes the equilibrium between the Fermi level and the energy of the surface adsorbed sites. Thus the energy levels of the surface state are limited with a value (qV_s) of approximately 0.5-1.0 eV which depends on the surface charge [92].

By solving Equation (2.2), it is possible to calculate the general surface barrier;

$$V_x = \frac{qN_d}{2\varepsilon_S} (x - x_o)^2 \tag{2.3}$$

where N_d represent the bulk donor density. By replacing N_d x_o by N_s (the density of electronic charge on the surface) the surface barrier will be,

$$V_S = \frac{qN_s^2}{2\varepsilon_S N_d} \tag{2.4}$$

which determines the electron energy required to reach the surface to be adsorb by oxygen [4].

From Equation (2.3), the width of the space charge region can be calculated from;

$$x_o = \sqrt{\frac{2\varepsilon_S V_x}{qN_d}} \tag{2.5}$$

The above result confirms that the space charge layer increase as the density of donor is decreased. The space charge region in also known as Debye length (λ_D) [93].

2.6 The Sensing Mechanisms

Two type of sensing mechanisms for semiconductors gas sensor has been suggested [6]. One that involves the change occurs in the bulk conductions, while the other includes the change in the surface conductions. The gas sensor that undergoes change in the bulk conduction is useful in the control of combustion process by measuring the oxygen partial pressure. This kind of sensors is usually works at high temperature (> 600 ^{o}C).

In this work, the second mechanism will be used to explain and model the results obtained, which could be briefly described as follows.

According to Barsan and Weimar [23, 24], the gas reaction with the metal oxide semiconductors can take place at different sites of the structure depending on the surface morphology. In the compact layer, the interaction with the gas takes place only on the surface of the semiconductor. This kind of layer can be realized through film deposition process such as sputtering and thermal evaporation. The second type of surface structure is the porous layer where the volume of the layer is accessible to the test gas. In this case the effective surface area is much higher than that of the former. This layer is the characteristic of the thick films which can be prepared by screen printing or by rheotaxial growth and thermal oxidation.

Properties of the metal oxide semiconductors depend on the chemical defects vacancies and interstitials. The vacancy refers to an empty (unoccupied) site of a

crystal lattice, i.e. a missing atom or vacant atomic site. The interstitial refers to an extra atom that may be lodged within the lattice of the crystal structure.

ZnO and other metal oxide semiconductors are well known as materials of high defects due to such as oxygen vacancies, zinc interstitial, zinc vacancies, and oxygen interstitial, where most of their electrical and optical properties are determined by these defects. Defects due to oxygen deficient is known to produce n-type electrical conductivity of the ZnO [44, 45, 49].

The defects must be in an equilibrium state, obeying mass, site and charge balance, where the ratio of anions (the oxygen in the case of ZnO) to cation of the crystal must be preserved, although the total number of sites can be increased or decreased, thus [16, 94];

$$Zn_{Zn}^{X} = Zn_{i}^{\bullet\bullet} + V_{Zn}^{''} \qquad (2.6)$$

where the left hand side of the reaction represents the initial state and the right hand side is the interstitial ($Zn_{i}^{\bullet\bullet}$) and vacancy ($V_{Zn}^{''}$) of the zinc. The valance state of the defects may vary; for the case of Zn interstitial in the ZnO, this can be $Zn_{i}^{\bullet\bullet}, Zn_{i}^{\bullet}$ and Zn_{i}^{X}. The same applies to the oxygen vacancies.

In the reduction state of the ZnO where there will be oxygen vacancies or zinc interstitial, in this case doubly or single charge defect can be written as [16, 94];

$$O_{O}^{X} = \frac{1}{2}O_{2}(gas) + V_{O}^{\bullet\bullet} + 2e^{-} \quad \text{or} \quad O_{O}^{X} = \frac{1}{2}O_{2}(gas) + Zn_{i}^{\bullet\bullet} + 2e^{-} \quad \text{(double)} \qquad (2.7)$$

or could be in the following

$$O_O^X = \frac{1}{2}O_2(gas) + V_O^{\bullet} + e^- \quad \text{or} \quad O_O^X = \frac{1}{2}O_2(gas) + Zn_i^{\bullet} + e^- \qquad \text{(single)} \qquad (2.8)$$

where O_O^X is the neutral oxygen from the surface, $V_O^{\bullet\bullet}$, $V_O^{\bullet}$ double and single ionized oxygen vacancy, $Z_i^{\bullet\bullet}$, $Z_i^{\bullet}$ are the double and single ionized zinc interstitials and e^- is the electrons from the conduction band energy level.

It was also found that substituting with foreign atoms enhanced the semiconductor properties (especially the optical and the electrical properties) of the ZnO, where the substitution of Zn atom alters the crystal properties depending on the concentration and the valance of the foreign atoms [95, 96].

As noted earlier, the change in the surface conductance of the semiconductor is affected by the presence of the gas which perturbed the equilibrium of the conduction reach by the material at constant oxygen pressure. The process of the oxygen adsorption at the surface is known to be dependent on the temperature. At low range temperatures (approximately less than 150°C) the process of the adsorption is known as physisorption where the bonding between the surface and the oxygen is by the Van der Waal force with small binding energy that causes an insignificant change in the electrical properties, where the oxygen is in its molecular form. This state acts as the precursor of the next state. At higher temperatures the oxygen ionic species participate in the interactions. These interactions produce a depletion layer at the metal oxide surface. This process is known as chemisorptions and occurs in the temperature range of 200 to 500 ^{o}C. In this type of reaction the binding energy exceeds 0.5 eV. Figure 2.6 shows the types of oxygen species detected at SnO_2 surface. It is well known that the oxygen molecules from the ambient are adsorbed at the surface of the metal oxide, subsequently converted to ions after capturing an

electron or two from the conduction band near, that depend on the temperatures, as represented by the following equations [97, 98];

$$
\begin{aligned}
&O_2(gas) \rightleftarrows O_2(ads) \\
&O_2(ads) + e^- \rightleftarrows O_2^-(ads) \\
&O_2^-(ads) + e^- \rightleftarrows 2O^-(ads) \\
&O^-(ads) + e^- \rightleftarrows O^{2-}(ads)
\end{aligned}
\qquad (2.8)
$$

where $O_2(gas)$ is the ambient oxygen, O_2^- is a single ionized oxygen molecules, O^- is a single ionized oxygen , O^{2-} is a double ionized oxygen and e^- is a conduction band electron captured from the surface. This explains the high resistance (low conductance) of the metal oxide sensors where the electrons are captured by oxygen which results in decreasing the carrier concentration of the material.

The presence of reducing gas such as hydrogen (H_2), methane (CH_4), ethanol (C_2H_5OH) and others near the surface of the sensor will result in a reaction between the adsorbed charged oxygen ions and the reducing gases which will release the captured electrons back to the conduction band of the sensor's material. Thus the carrier's concentration is increased that caused the sensor resistance to be decrease. The following equations demonstrate these behaviors.

$$
\begin{aligned}
&R + O^- \longrightarrow RO + e^- \\
&\text{or} \\
&R + O^{2-} \longrightarrow RO + 2e^-
\end{aligned}
\qquad (2.9)
$$

where R is a reducing gas. The decrease of the sensor resistance would be proportional to the amount (concentrations) of the target gas.

For oxidizing gas such as ozone (O_3) and nitrous (NO_x), the oxygen from the gas will attract more electrons from the conduction band of the sensor material that will reduce the carrier's concentration and as a consequence increase the resistance.